Applicability of Heat Pipes and Impingement Cooling for Axial Compressor Tip Clearance Control

A Preliminary Investigation

Guilherme M. Luz
guilherme.luz@tum.de
Volker Gümmer
Technical University of Munich
Institute of Turbomachinery and Flight Propulsion
Munich
Germany

Abstract

This publication presents the results of a numerical analysis aimed at assessing the applicability of thermal tip clearance control (TCC) to the fore-to-last stage of a 10-stage high-pressure compressor system. The chosen geometry is representative for the HPC rear stages of a modern middle-sized turbofan, designed for large business jets and regional airliners. Simplified models for two TCC concepts were implemented isolated and in combination: external impingement cooling and heat pipes. The analysis was performed by means of finite-element thermostructural simulations. Transient operational cycles, derived from a meanline model, along with empiric correlations for heat convection provided the required boundary conditions. Qualitative similarity to selected previous works in terms of temperature, stress and clearance evolutions was achieved. The combination of concepts demonstrated its potential as a TCC system with up to 0.45% reductions in rotor and stator clearances. Calculated heat pipe temperatures and heat fluxes were inside the estimated operational limitations. Regarding stresses, some local concentrations were observed, without significant impact in critical stress regions. A slam cycle analysis showed that, while blade rubbing remains a possibility, it can be mitigated by robust cooling control. All in all, the concept was deemed worthy of more detailed studies.

Keywords: Tip Clearance Control; Axial Compressor; Heat Pipes; Impingement Cooling.

NOMENCLATURE

Latin Symbols and Acronyms

A	Cross-sectional Area
ADP	Aerodynamic Design Point
C_d	Discharge coefficient
D	Diameter
E	Elasticity modulus
EGT	Exhaust Gas Temperature
FEM	Finite-Element Method
h	Blade height
HP	Heat Pipe
HPC	High-Pressure Compressor
HPT	High-Pressure Turbine
k	Thermal Conductivity
L	Length
$\dot{m}$	Mass Flow
Ma	Mach Number
Nu	Nusselt Number
p	Pressure
Pr	Prandtl Number
R	Gas Constant, Radius
Ra	Rayleigh Number
Re	Reynolds Number
s	Tip gap height
t	Thickness
T	Temperature
TCC	Tip Clearance Control

Greek Symbols

α	Convective HT coefficient
ϵ	Surface Emissivity
κ	Isentropic exponent
σ	Stress

Sub- and Superscripts

a	Adiabatic
c	Condensator
e	Evaporator
ex	External
i	Inner
is	Isentropic
j	Jet
o	Outer
pl	Plenum
s	Static Value
t	Total Value

1 INTRODUCTION

Improved gas path sealing has been an active field of development ever since the first gas turbine engines were designed. The impact of tip clearances on engine performance and lifespan has stirred interest on blade tip sealing techniques already from the 1960's [1]. At first, clearance control systems were mostly investigated for the engines's hot end (the HPT), given potential positive effects on component life. With tighter clearances, an engine is capable of delivering the same thrust at a smaller EGT, which in turn results in longer time spans between required maintenance rounds. In 1979, Kawecki [2] published an extensive study of turbine TCC concepts for transport and military applications. His conclusions show the positive impact of such systems over the overall life-cycle costs of an engine. Along with blade cooling systems, turbine TCC has been established as standard in modern engines.

The development of TCC systems for the cool side of the engine (HPC) has followed somewhat different trends. It is established that tip leakage losses play a significant role on compressor efficiency and stability. 1% extra clearance can represent up to 2% less isentropic efficiency and 7.5% in surge margin [3], [4]. However, the additional costs and complexity inherent to such systems has hindered past interest on them [2]. On a time in which significant improvements in engine performance were still tangible by simpler measures (e.g. improved aerodynamic design, faster rotating machines), it did not make sense to pursue relatively expensive solutions. Attention to TCC modeling rose from the 1980's. Research on simple, fast-running models for tip clearance has since then been developed [5], [6], [7]. Among the goals stood correcting overall preliminary design and performance models by considering transient clearance changes. More recently, interest in TCC for HPC's has been renewed and more extensive work was performed. Some examples are the work of Rockel et al. [8], and Schmidt et al. [9] in auxetic structures for influencing compressor tip sealings, a passive mechanical solution with limited potential. Other proposed solutions involve aerodynamically influencing tip flow so as to reduce the effective flow area, both by active inflow control [10] and recirculation [11]. On the thermal side, Horn [12] assessed air impingement for the HPC over the operational behavior of a turbofan. Also Schmidt [13] preliminarly investigated a casing cooling design with embedded heat pipes for the HPC. Horn's work performed a very simplified analysis, with focus on the influences of clearances over the compressor operational lines

by means of an idealized cylindrical casing geometry. Schmidt focused on TCC metamodelling for fast preliminary design calculations. More detailed investigations were not performed.

To the extent of the authors' knowledge, thermal TCC for compressor systems is still a scarcely investigated topic. The present work aims to shed some light on it by presenting a preliminary analysis of selected concepts. For this purpose, a rotationally-symmetric FEM-model was developed considering a geometry representative for the HPC rear stages of a modern middle-sized turbofan. Properties at different operational points were calculated using the commercial performance tool *GasTurb*® [14]. Secondary flow properties were estimated following the approach described by Sultanian [15]. By means of correlations available in literature (see [16], [17]), heat transfer was modeled. An in-house developed tool allows flexibly creating transient cycle curves for various investigation purposes. Two thermal TCC concepts, impingement cooling and heat pipes, were then implemented and their isolated, as well as combined effects over the structure were assessed.

This work starts by presenting the considered test geometry, the numerical setup and associated boundary conditions. Then, first results for a square-like test cycle are presented and a comparative discussion with selected literature sources is made to qualitatively demonstrate the model's ability of reproducing transient temperature, stress and clearance evolution trends. The influence of the different concepts, isolated and combined is discussed and parametric studies regarding heat pipe distribution and cooling magnitude are presented. The combined concept is then tested under a slam deceleration-acceleration cycle to assess its effect on a critical transient. Finally, conclusions and an outlook to future work wrap up the written piece.

2 MODEL SETUP

2.1 GEOMETRY AND OPERATIONAL POINTS

An HPC representative geometry of a commercial twin-spool engine was selected as the study object. Similar machines are currently in-service on large business jets, as well as regional airliners with up to 80 passengers. Figure 1 depicts a cut view of the machine. Following the considerations made by Rockel et al. [8], rotor 9 was chosen to be modeled. The fact that it is far from the vortex reducer and the rear cone enables simplifying the model to a single blisk fixed to the surrounding structure by its lateral flaps. For the casing, it was decided to model the complete double-walled structure between the two external flanges. This follows the approach of Schmidt et al. [18], which simplifies structural fixation, besides leaving room for TCC features. Lattime and Steinetz's review [1] shows that axisymmetric thermal and mechanical loads are responsible for at least 70% of total clearance changes. DeCastro et al. [19] set tolerances on clearance control related to asymmetric effects at around 15% of total clearance changes. Based thereon, modeling only axissymmetric loads and setting a minimal tolerance for clearances should suffice to adequately represent tip clearance behavior. This also justifies the adopted simplification of a rotationally-symmetric model. Only a sector of 10° was modeled. The simplified geometry is exhibited in figure 2. The decision to remove flange screws was based on the findings of Schmidt et al. [20]. Namely, bleed-air ports and flange screws have a negligible contribution to clearance-relevant displacements. Naturally, removing the screws and tying the flanges to one another will have an impact on

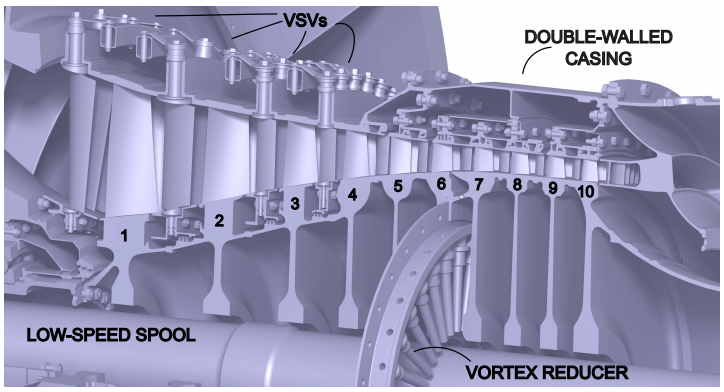

Figure 1: Cut view of representative HPC chosen for the study.

local stress distributions. Those are however not primarily relevant for the present analysis. Finally, it was necessary to determine the material from which the structures are built. Based on Schmidt's discussion [13], INCONEL718 was chosen as the main alloy for the structure and NiCoCrAlY for the rotor coatings. Mechanical properties were taken from previous works (see [21], [22], [23], [24]) and a technical sheet [25].

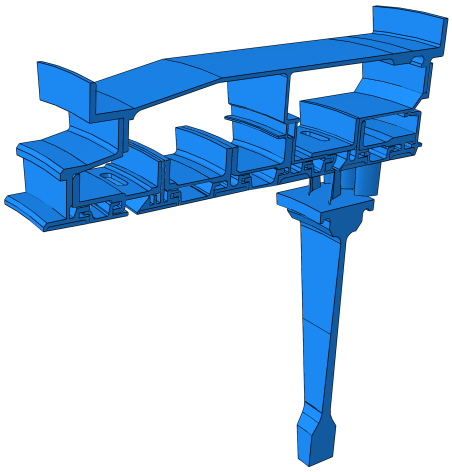

Figure 2: Perspective view of modeled geometry.

Regarding operational data, little is generally available in open literature. At most, operational limits are available in engine certification sheets [26]. This information, along with guidelines adopted by previous works (see [13], [8]) oriented the values assumed for the design point. Off-design data, detailed engine station data, as well as meanline data for the HPC were then calculated by means of the commercial performance tool *GasTurb*®. Besides meanline properties, it was necessary to estimate the properties of relevant secondary airflows. Only then it became possible to simulate the structure's thermal behavior. For this purpose, the airflows were modeled as inefficient polytropic expansions, considering the discussions of Sultanian [15]. For the transients, it was necessary to model the time evolutions of all involved variables. There is in reality a two-way coupling between structure and surrounding fluid flows, for which sophisticated models are required. This would be an impossible task with the available resources, so a simplified approach was adopted. Merkler et al. [5] discuss the transient behavior of a HPC rotor disk and provide some details on the relaxation times for temperatures at different locations. Based on that, the transients were modeled by means of logarithmic functions whose coefficients depend on the prescribed relaxation times.

2.2 NUMERICAL MODEL AND BOUNDARY CONDITIONS

The numerical model consists of a FEM implementation in the commercial software *Abaqus*®. Given the relatively small displacements, a one-directional coupling between the energy and the stress-displacement equations was assumed. This allows sequentially solving the transient heat transfer problem and then inputting the solution into the structural simulation, rather than solving a two-way coupled problem. The main advantages are the robustness of the solutions and the reduced computational times. The same approach was used by Rockel et al. [8] and Schmidt et al. [20]. The domain was discretized in fully-integrated, quadratic elements. Element shapes and mesh structure varied according to the expected stress levels and geometry complexity. For the rotor, tetrahedral elements were used, with a total of 245482 nodes. For the casing, a mixture of structured and swept, unstructured meshing was applied. Elements were set as hexahedral, with some exceptions in the swept regions of more complex geometry, such as stator 9. A total of 492415 compose the casing mesh. An overview of the generated meshes is provided in figure 3. A grid study was performed to ensure numerical accuracy while maintaning the simulation times as fast as possible.

Contact modelling was required between the various parts of the casing structure. Surface-based interactions were chosen with different properties, based on the nature of contacts (screwed, mounted, rolling). The model was supplied with static pressure loads, surrounding flow temperatures, surface emissivities and convective heat transfer coefficients. The approach was based on the work of Horn [12] and Rockel et al. [8]. A comprehensive overview of the considered thermal boundary conditions is provided in figure 4, along with a summary of relevant correlations in table 1.

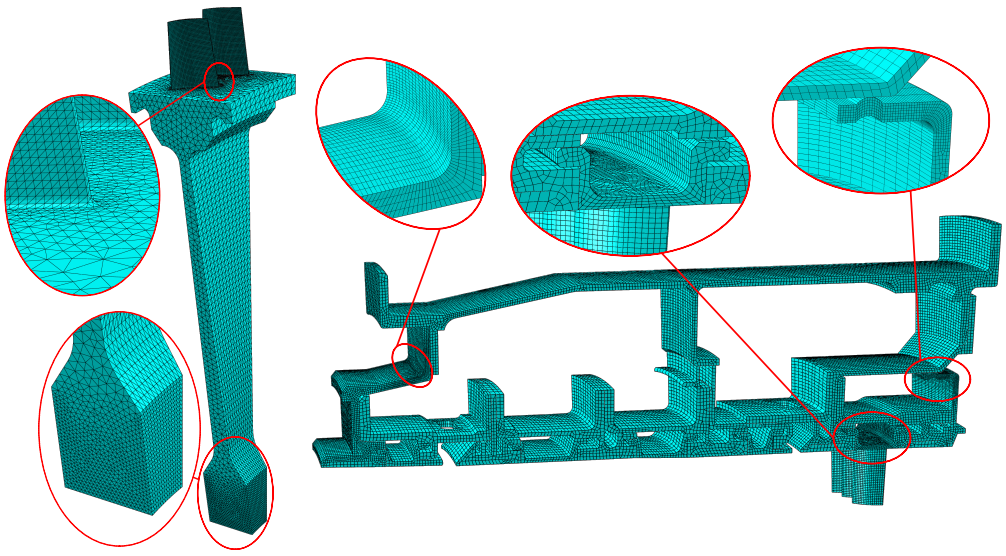

Figure 3: Reference meshes for rotor (left) and casing (right).

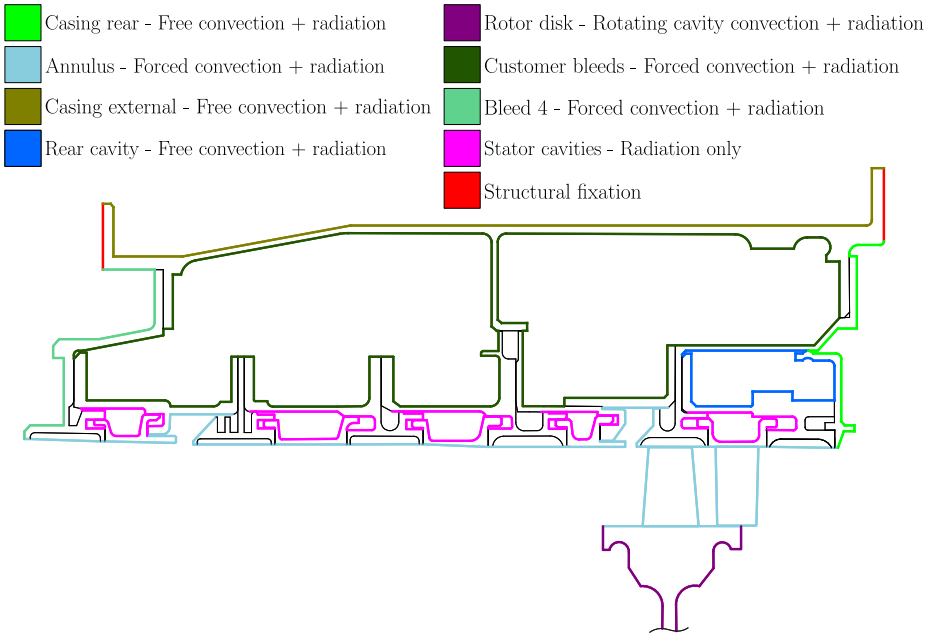

Figure 4: Meridional view of domain with considered BC's. Static presures were also modeled for all surfaces.

Radiation was considered by applying built-in implementations available in *Abaqus*®. Based on the findings of Keller et al. [27], $\epsilon = [0.1;\ 0.6]$ is reasonable for INCONEL 718. Inside this range, the emissivity was set to 0.2 after preliminary simulations revealed marginal influence. This is in line with previous findings, which support the relatively small role of radiative (10%-15%) compared to convective heat transfer inside a compressor [28]. From Tirovic et al. [29] and Jalalpour et al. [30], the range for flange contact conductances in high-performance engineering applications should be about 2000-20000 W/(m^{2}K). The conductances

Boundary (Source)	**Nu Correlation**
Main annulus (Horn [12])	$0.0214Pr^{0.4}[Re^{0.8} - 100]$
Blades (VDI Heat Atlas [17])	$\frac{0.037Re^{0.8}Pr}{1+2.443Re^{-0.1}[Pr^{2/3}-1]}$
Rotor disk (Alexiou et al. [16])	$6.9386\times10^{-6}{Re_z}^{1.301}\left(\frac{r}{b}\right)^{-3.523}$
Customer bleeds (VDI Heat Atlas [17])	$0.0214Pr^{0.4}[Re^{0.8} - 100]$
Casing external surface (VDI Heat Atlas [17])	$0.15[(1+2Pr^{-9/16})^{-4/9}]^{4/3}Ra^{1/3}$
Casing rear surface (VDI Heat Atlas [17])	$0.42Pr^{0.012}Ra^{0.25}\left(\frac{h}{l}\right)^{-0.25}$
Casing rear cavity (VDI Heat Atlas [17])	$0.2Ra^{0.25}\left(\frac{R}{r}\right)^{0.5}$

Table 1: Summary of adopted correlations for convective heat transfer over the structure.

were set to 2000 W/(m^{2}K), after initial calculations revealed again marginal changes in overall response for higher values.

3 TIP CLEARANCE CONTROL CONCEPTS

3.1 EXTERNAL IMPINGEMENT

The impingement concept was conceived based on current systems present in low-pressure turbines of typical turbofan engines. The system consists of bleeding cool air from the bypass and impinging it over the structure. A conceptual sketch of it is presented on figure 5. The main feature of this concept is to create a localized area of high heat transfer at the expense of little bled mass flow. Another attractive feature of external impingement is its easy integration to existing geometries without the need for major restructuring, required to isolate the various flows at different pressure levels inside the casing. In order to characterize the system, a model was created using the correlation available in Florschuetz et al. [31] for the Nusselt number and the corrections by Goodro et al. [32] for higher Mach numbers. Given a jet diameter (D_j) and thermodynamic state of the fluid inside the distribution box ($p_{t,pl}$,$T_{t,pl}$), all other relevant quantities can be calculated. That is, jet Reynolds and Mach numbers (Re_j, Ma_j), jet static pressure and temperature ($T_{s,j}$, $p_{s,j}$), and the jet mass flow ($\dot{m}_j$). Pressure losses and jet velocities are a function of the discharge coefficient, defined as the ratio of isentropic to real mass flows [33], or

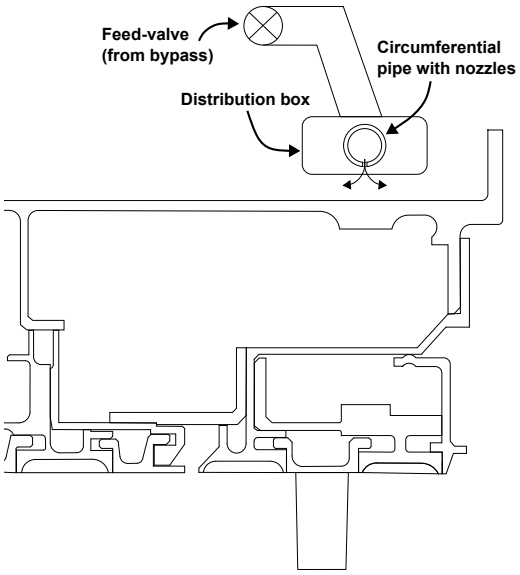

Figure 5: Conceptual design of impingement system.

$$C_d = \frac{\dot{m}_j}{\dot{m}_{j,is}} \tag{1}$$

where

$$\dot{m}_{j,is} = A_j \frac{p_{t,pl}}{\sqrt{RT_{t,pl}}} \left(\frac{p_{ex}}{p_{t,pl}}\right)^{\frac{1}{\kappa}} \sqrt{\frac{2\kappa}{\kappa-1}\left[1-\left(\frac{p_{s,j}}{p_{t,pl}}\right)^{\frac{\kappa-1}{\kappa}}\right]} \tag{2}$$

For the present work, the free design variable for the impingement system is the jet diameter. The total pressure and temperature are fixed by the available air in the bypass. Figure 6 displays the calculated impingement jet properties. The system is feasible as long as the jet static pressure is above the static pressure of the medium where the flow is impinging, which proved to be the case for all investigated diameters. From the results, smaller nozzles are more favorable. Considering the heat pipe design exposed in the next section, another restriction is that the complete condensator area is cooled by the impingement system. Therefore, the diameter is set to 3mm, also to ensure a static pressure safety margin. At this diameter, α_j=321.1 W/m^{2}K, $\dot{m}_j$=0.57 g/s, N_j=130 for a $\dot{m}_{j,total}$=74.13 g/s of impingement air. Considering the estimated mass flow of 70.46 kg/s for the bypass, the amount of required bleed air lies at 0.11% and is negligible in terms of lost fan thrust.

In the FEM model, the impingement cooling is implemented as a surface boundary condition with the given temperature and heat transfer coefficient. The number of jets, as well as the surface area impacted are determined considering that the pitchwise distribution of jets and the axial averaging length of Nu_j is equal to $5\times D_j$.

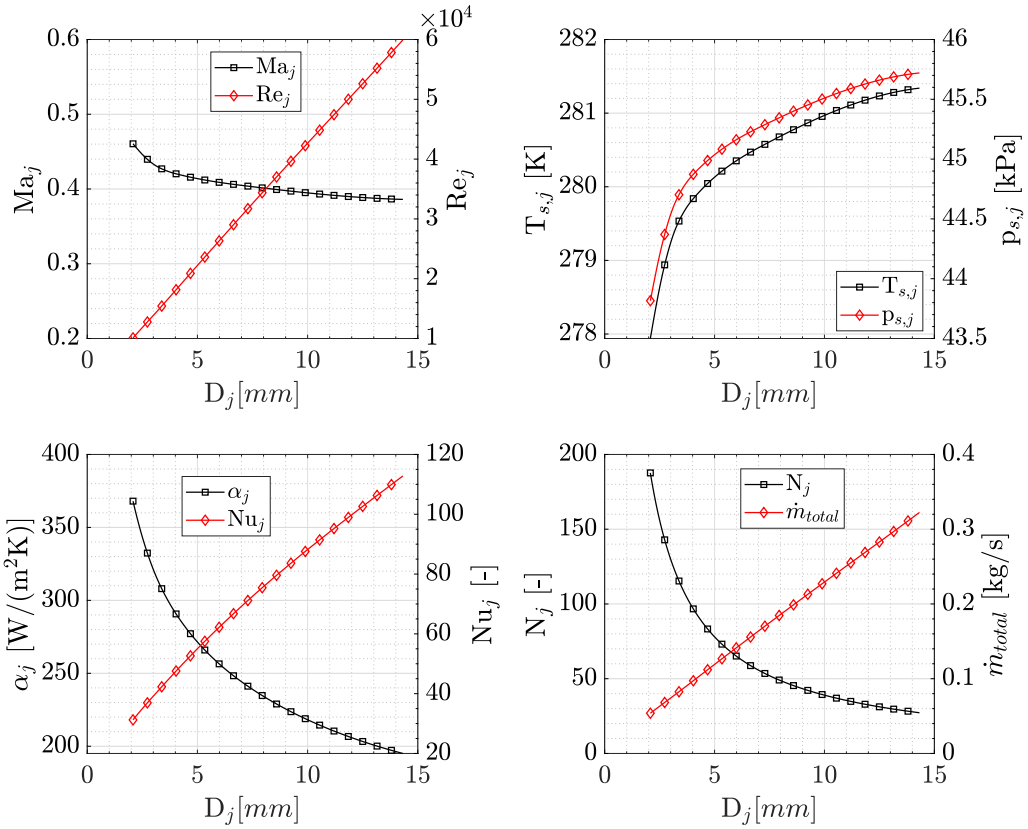

Figure 6: Impingement jet properties for fixed feed-flow conditions (cruise-flight). Parameter range for which the model is valid: Re ∈ [10000,60000]; Ma ∈ [0.2,0.6].

3.2 CONCENTRIC ANNULAR HEAT PIPES

Concentric annular heat pipes provide improved anti-gravity operation when compared to conventional designs. This is due to the extra wick area made possible by the presence of the inner pipe wall. The design considered in this work is inspired by Zhao et al. [34], who also proposed a composite wick design to increase the capillary limit even further for a high-temperature concentric annular heat pipe. The conceptual design of the heat pipes applied in this work is depicted in figure 7, as well as the main associated dimensions.

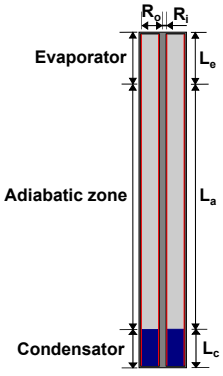

Parameter	Value
R_i $[mm]$	0.5
R_o $[mm]$	4
L_e $[mm]$	4.3
L_a $[mm]$	46
L_c $[mm]$	7
t_p $[mm]$	0.5
Filling ratio	25%
Working fluid	*Dowtherm*® A
Wick structure	400-200 mesh composite screen wick [34]

Figure 7: Conceptual design of the concentric annular heat pipe.

From Noda et al. [35], a model for the screen wick properties was derived. The results were modified to include the improvements achieved by Zhao et al. [34]. Using the modelling approach described by Chi [36] and Faghri [37], and applied by Nemec et al. [38], the operational limits of the heat pipe design were calculated. The geometric dimensions of the heat pipe were set within the limits of structural accomodation on the reference casing geometry. Material properties for the working fluid were taken from Faghri et al. [39],[40]. With all the parameters defined, it was possible to calculate the operational envelope of the heat pipe. It is displayed in figure 8 for the case in which the heat pipe is operating against gravity (i.e. the most unfavorable condition). The internal stresses were also estimated using a simple pressurized pipe model, as defined by Faghri

[36]. Given the proposal of manufacturing the heat pipes with the same material as the casing, the estimated values are well below any material limits and were not taken as cause for concern.

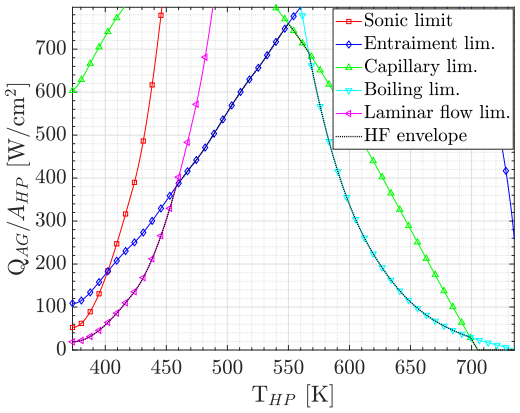

Figure 8: Heat pipe calculated operational envelope for anti-gravity operation.

The heat pipes are implemented in the FEM model as individual parts composed of two different materials. The container volume is modeled as INCONEL718, with exactly the same thermomechanical properties as the casing structure. The inner volume of the heat pipe is modeled following the approach adopted by Eisemann et al. [41]. That is, to consider the inner heat pipe material as having a small elasticity modulus (taken as E=10 MPa), a very high thermal conductivity (k=20000W/m.K), a density and specific heat which corresponding to the mass average of working liquid and vapor, both temperature-dependant. The thermal expansion coefficient is taken as the same as for the container. That way, the high heat flow can be simulated and non-physical effects caused by thermal expansion and mechanical stress transmission are avoided. The overall heat pipe conductivity is then mainly a function of the container thickness and the wall area over which heat is transferred, which is automatically handled by the FEM solver. For the considered model, the estimated mass of one heat pipe lies at 4.7g. If they are placed circumferentially at a 5° pitch (72 units), the total added weight is 338.4g. In comparison, copper bars with the same volume would weight in total 1.86kg, roughly 5.5 times more.

4 RESULTS AND DISCUSSION

4.1 SQUARE CYCLE ANALYSIS

Although the lack of experimental data makes proper validation an impossible task, a qualitative comparison with selected literature sources was performed. For the rotor, temperature and stress evolutions for a squarecycle (IDLE-MTO-IDLE) are presented in figure 9. The results of Merkler et al. [5] were used as a reference for the comparison. Given that different geometries are considered and that the reference data is not plotted in absolute terms, only trends can be compared. In general, the results are satisfactory. The stress evolutions show correct trends, with compression on the rim (red curve, lower graph in figure 9) during the acceleration phase , followed by stabilization at an adequate difference between stresses in different rotor heights. Relatively high bore stresses are observed, which is attributed to the fact that the rotor is simplified as a blisk. The extra mass filling the blade posts adds up to the centrifugal forces being transmitted to the bore. Regarding temperature distributions, the curves are closer together than for the reference, which is due to the fact that the bleed air comes not from the compressor inlet as for the reference, but from stage 6 and is thus hotter.

For the casing structure, even qualitative comparisons in terms of temperature and, or stress evolutions are impractical, due to the myriad of different flange geometries. Therefore, the casing response was tuned based on the resulting tip clearances. Figure 10 exhibits the calculated clearance evolution for a similar square cycle. The results of the selected literature source (see [6]) are not reproduced here, the reader is invited to make the comparison. Referring to the deceleration from MTO to IDLE (2000s), the fast opening caused by the reduced centrifugal forces is followed by a closing caused by the casing cooling. The rotor blisk, more massive, takes longer to cool. Its cooling leads to the final clearance opening towards the stationary level.

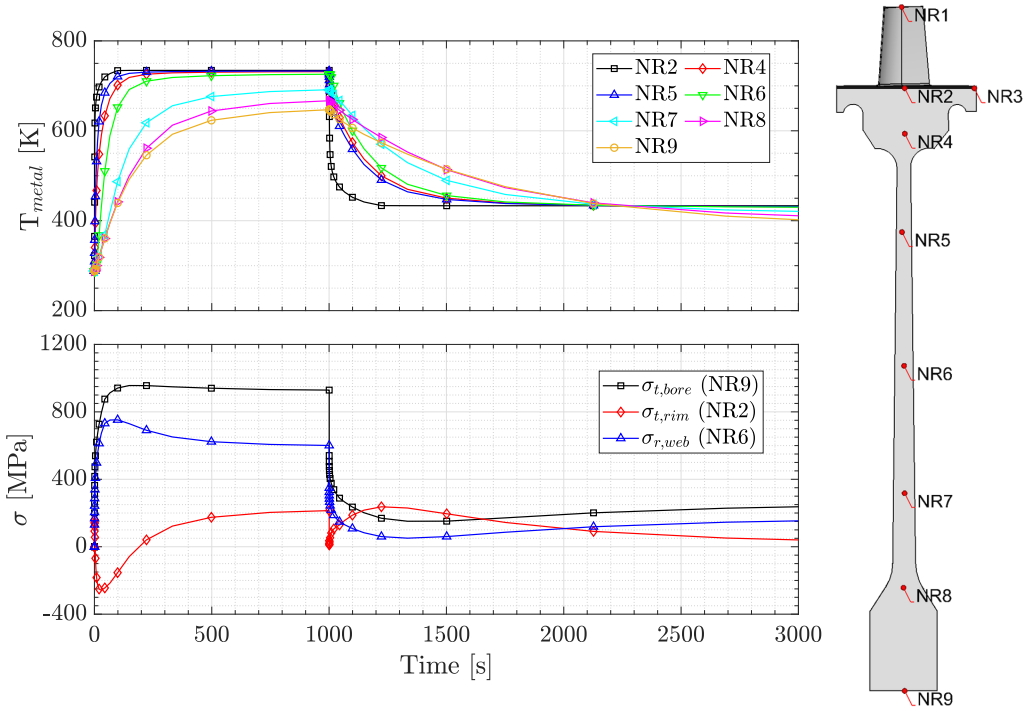

Figure 9: Temperature and stress evolutions for the rotor disk for a square test cycle (left). Reference measuring nodes (right). The time span was adjusted to match the curves displayed by Merkler et al. [5].

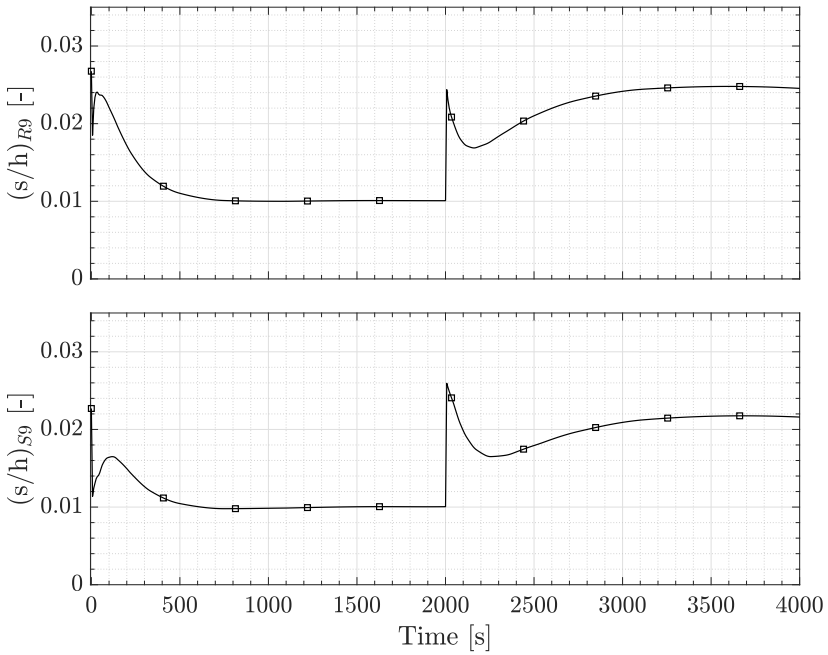

Figure 10: Calculated tip clearances in stage 9. The time span was adjusted to match the curves displayed by Schulte et al. [6].

4.2 INFLUENCE OF IMPLEMENTED TCC CONCEPTS

For evaluating the concepts, the test cycle consists of an acceleration to MTO until a stationary regime is reached followed by a deceleration to steady ADP conditions. The whole cycle consists of 4000s, 1500s for the MTO phase and 2500s for the ADP one. The impingement system is turned on 300s after the start of the ADP phase. Figure 11 exhibits the FEM implementation of the concepts. Notice the position of the proposed heat pipe fixation in the structure, between stator 9 and rotor 10.

In figure 12, the transient clearance curves of the different concepts. Some effects are observable. Firstly, the heat pipe decelerates the casing response to the new operational point conditions. That is reflected by a lower clearance peak after the initial pinch point at the beginning of the MTO phase ($\sim$ 100s). Regarding ADP clearances, isolated concepts had no effect whatsoever. For the external impingement, this was expected, given the local cooling action. For the heat pipes, some appreciable effects were expected, however not seen. As it will become clear further in this work, the condensator cooling magnitude, the position and quantity of heat pipes have a defining effect over their influence. In fact, the combined concept implementation already shows this. A very small clearance reduction was achieved for the rotor (1.69% to 1.59% or 0.1%). For the stator, the effects are more pronounced (1.60% to 1.31% or 0.29%). Still, a relatively small influence.

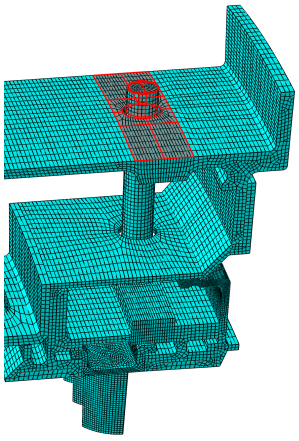

Figure 11: 10° pitch HP concept. In red, impingement BC surface.

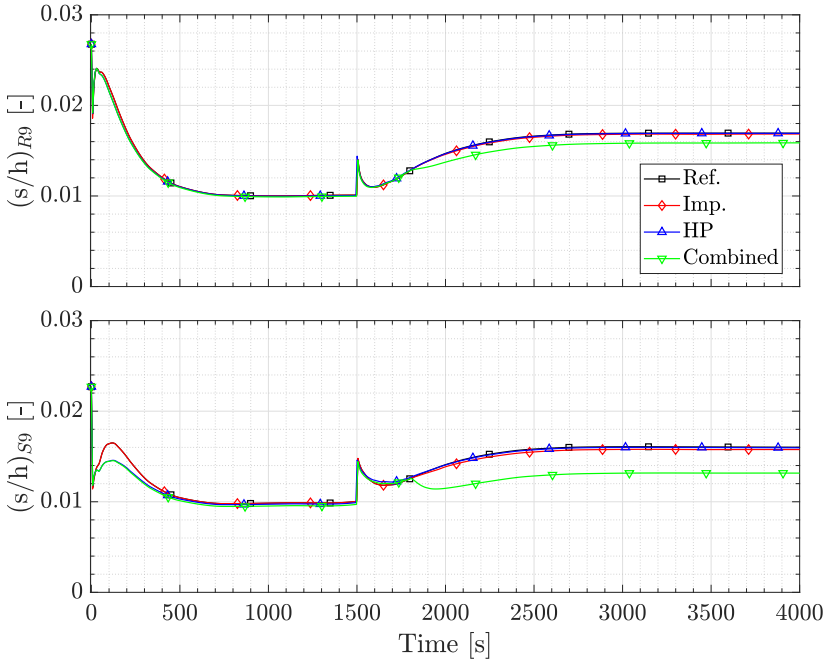

Figure 12: Clearance evolutions for implemented concepts.

Figure 14 displays the *von-Mises* stresses for the critical region of the casing at cruise. The tendency to "bend" forward due to the higher temperatures at the rear part generates the highest stresses at the front flange. For the reference, they reach 861 MPa for the MTO phase and level out at 632 MPa for cruise conditions. While the heat pipe along does not have appreciable effects over the critical stresses, the external impingement scheme actually reduces them to 494 MPa. This is due to the overall temperature reduction at the rear casing section. Naturally, there is a redistribution of stresses, not shown here, to other flanges at the rear part. However, the absolute stress values remain lower than the critical one. There is only one exception to this, at the bore introduced on the outer casing structure to accommodate the heat pipe. The expected geometry-induced stress concentration is enhanced by the large temperature difference caused by the impingement system, which leads to stresses up to 892 MPa at cruise. The corresponding contours are displayed in figure

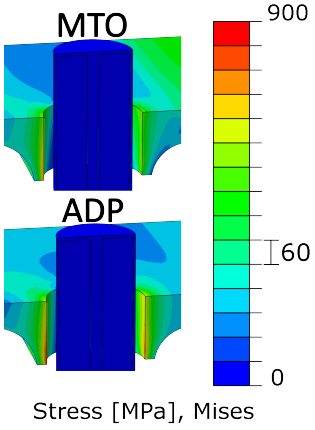

Figure 13: Stress concentration at heat pipe bores.

13. A possible solution for this issue could be achieved by thermally isolating the casing structure under the impingement jets, so that the cooling effect is restricted to the HP condensators.

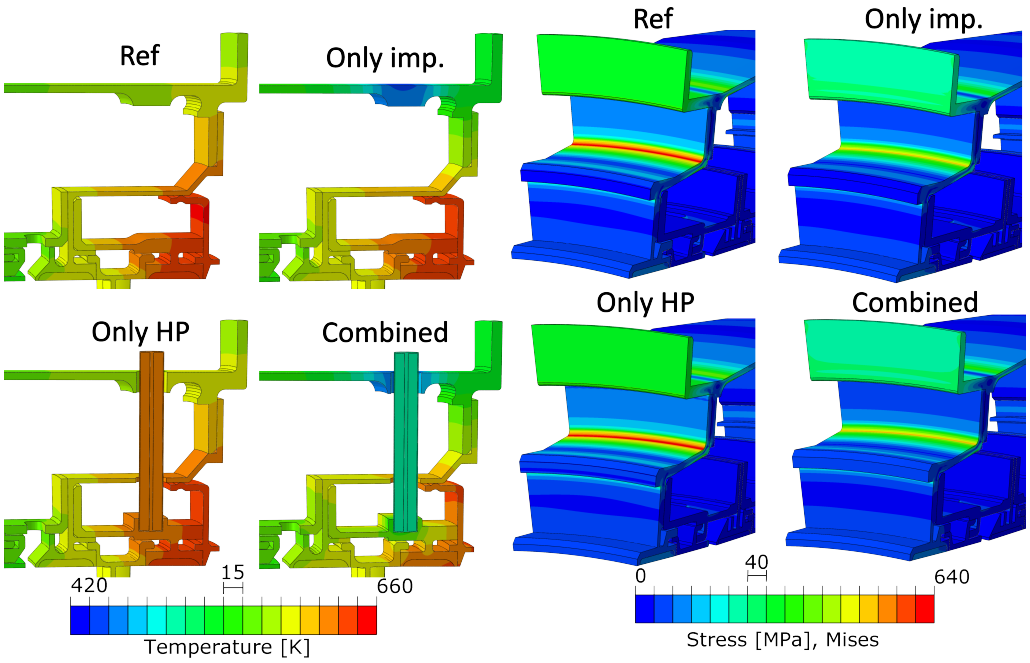

Figure 14: Temperatures at rear part of casing (left) and *Von-Mises* stresses in critical region (right) for the implemented concepts.

One last aspect worth mentioning relates to figure 8, the operational envolope of the heat pipe. At ADP, the heat pipe's temperature remains almost constant at 502 K. During the MTO phase, without cooling, it rises to 744 K. For the first condition, the maximum heat flux inside the heat pipe reaches 43.9 W/cm^2. For the last, it stays at 7.4 W/cm^2. Considering the calculated operational envelope, dry-out should occur for the MTO condition, while safe operation seems feasible for the ADP phase. Whether exposition to such high temperatures is an issue or not requires further investigation. Two main aspects here are the recuperation of dry-out and working fluid decomposition. Considering dry-out, Baraya et al. recently showed the possibility of normal operation restablishment, with some temperature hysteresis [42]. For the intended operational point, the heat pipes can still be considerably pushed to lower temperatures to allow increased heat flux.

4.3 INFLUENCE OF HP DISTRIBUTION

Considering the local influence of the heat pipes and the direct dependency between flange temperature and displacement (i.e. clearance), the influence of increasing the quantity of heat pipes (reducing the pitch), as well as the effects of changing their attachment position to the structure were investigated. For clarity, the FEM implementation for the 5° at the frontal position is displayed in figure 15. They are fixated between both vanes of stage 9, so as to have local action over the coatings of rotor 9.

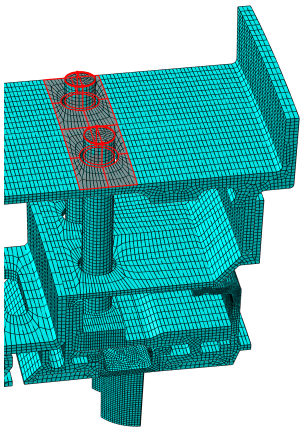

Figure 15: 5° pitch HP concept. In red, impingement BC surface.

The obtained clearance curves are summarized in figure 16. The effect of positioning the heat pipes closer to the rotor is evident by comparing the respective curves (green and cyan). Rotor 9 clearances go from 1.69% to 1.50% to 1.24% considering the reference, 5° pitchwise rear and front positionings, respectively. This means a reduction in 0.29% and 0.45% clearance for the same impingement cooling. There is some penalty in the stator 9 clearances, from 1.09% to

1.17% (or 0.08% increase) when moving the heat pipes axially towards the rotor. In essence, the benefits outweight the costs. Additionally, these results further confirm the local action of the cooling system. Regarding the quantity of heat pipes, the results are quite intuitive. The more heat pipes, the more heat transfer, the lower the temperatures and therefore, the tighter the clearances.

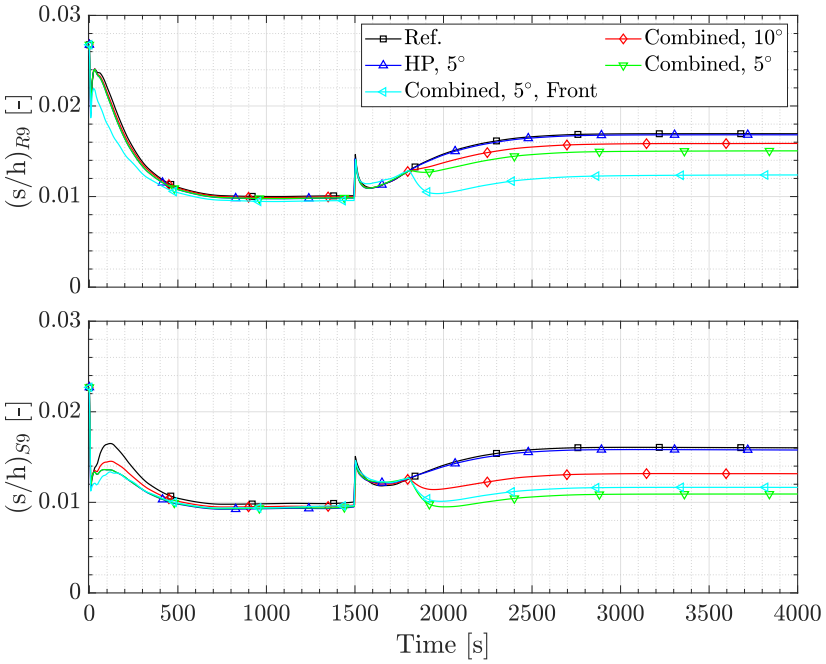

Figure 16: Clearance evolutions for different pitchwise and axial distribution of heat pipes.

Regarding stresses, the modified configuration exhibits a similar behavior to that discussed in the previous section. The peak stresses at the casing front flange increase by little, going to about 878 MPa. The heat pipe bore holes added to cooling cause a stress concentration. However here, an additional benefit of the different heat pipe positionining becomes evident. The generally lower stress level at the front position lead to lower concentrated stress at the bores, as displayed in figure 17, with peak of 601 MPa on the bores for the ADP phase.

The last aspect relates to safe heat pipe operation. The discussion is similar as before, for the 10° pitch case. The operational temperatures go up to 788 K during the MTO phase, with a reduced heat flux of only 3.5 W/cm^2. During the ADP regime, HP temperature stabilizes at 471 K with a heat flux of 37.7 W/cm^2. Also for this configuration, the improvement potential through enhanced condensator cooling is evident. Dry-out and working fluid decomposition during critical operation might pose an obstacle to an actual implementation.

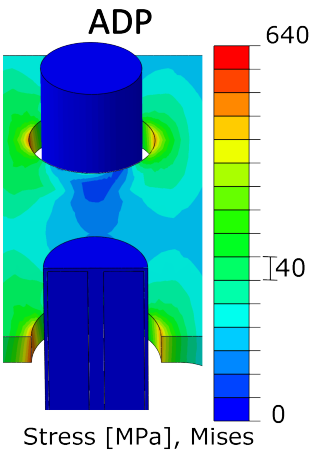

Figure 17: Stress concentration at heat pipe bores for the 5° pitch, frontal configuration.

4.4 INFLUENCE OF COOLING MAGNITUDE

Building up on the previous discussion on the available operational envelope for cruise conditions, the impingement cooling was artificially enhanced to assess its influence over the system's response in terms of clearance. Figure 18 depicts the steady clearances at cruise for different impingement heat transfer coefficients. There is a slight tendency towards saturation, expected as the temperature of the heat pipes approach that of the cooling air. The right side of figure 18 clarifies the tendency towards saturation. The theoretical limitation is to have a large enough cooling to equalize heat pipe and impinging

air temperatures. Considering T_j=279.2 K, the required magnitude of α_j would make it impractical to reach this lower limit, and already at the tested levels, the benefits become marginal when compared to the corresponding cooling enhancement. This is naturally a very simplified first assessment. Relatively simple cooling enhancement techniques, such as adding fins to the heat pipe condenser, might be worth more attention.

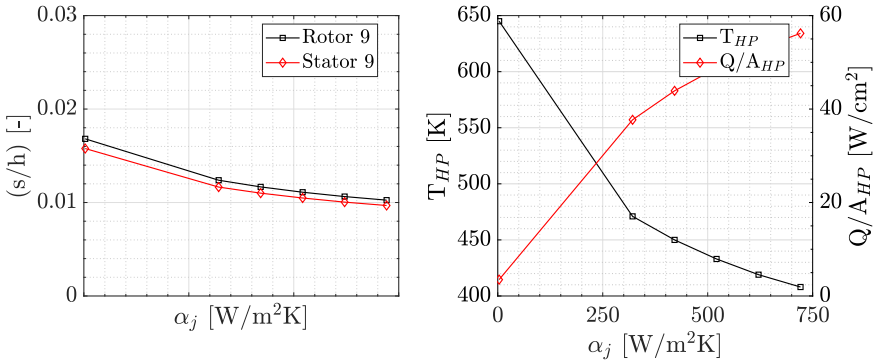

Figure 18: Variation of ADP clearances, HP temperature and max. heat flux with α_j.

4.5 CLEARANCES UNDER SLAM ACCELERATION

As a final round of assessment, the system's behavior was analysed under a strong transient which could potentially bring the rotor blades into rubbing danger. The test slam cycle comprises an stabilization in cruise conditions (ADP) followed by a deceleration to high-altitude idle (HIDLE) for 100s and a consecutive acceleration to the top-of-climb condition (TCL) over another 100s, then followed by a restabilization in ADP. Provided the impingement system is on only during the cruise phase, this transient slam cycle reflects a situation where the aircraft is required to descend for a short period and then suddenly ascend again, for example as a dodging manouver to avoid incoming air traffic. Other common critical transients, such as an aborted landing, are not adressed, because the system would not be active during this flight phase. Only the combined concept with 5° HP pitch and frontal positioning was simulated (see figure 15). Two control cases were investigated for the impingement system. The first one was to simply leave it on during the whole transient manouver. The second involved turning off the system at the start of the deceleration and turn it on after 100s of stable cruise regime. The respective results are shown in figure 19.

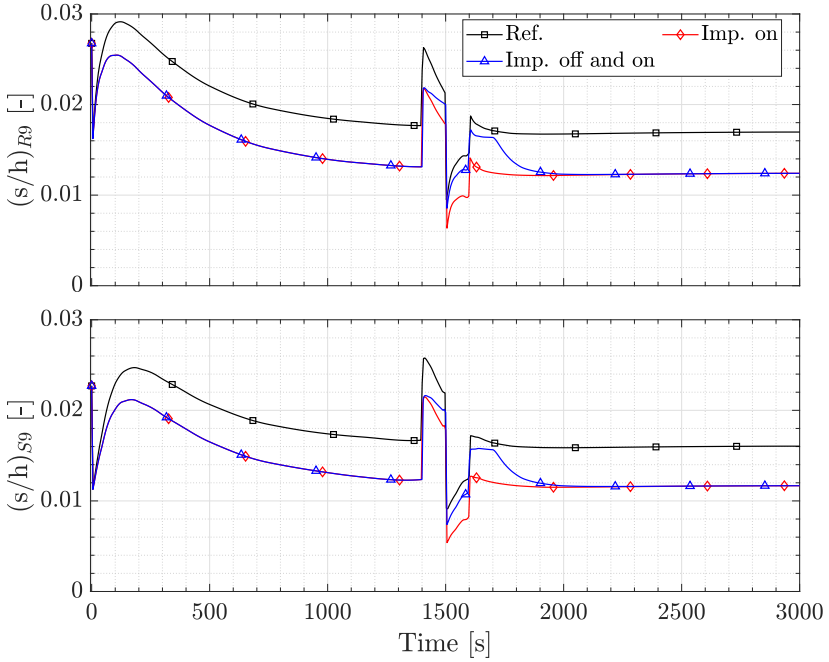

Figure 19: Clearance evolutions for high-altidute slam transient cycle.

The system's influence over the transient is noticeable for the continously on case. Pinch clearances reach a value as low as 0.63%. For the reference, the minimum clearance is 0.98%, quite close to the steady MTO one. Turning the system off improves the critical clearance in 0.24%, with a minimum of 0.87%. The stator shows a similar trend, with 0.90% for the reference compared to 0.54% for the continous impingement case and 0.74% for the off-on case. Although conclusions on rubbing cannot be drawn at this point, the model shows that a robust control system can mitigate transient rubbing dangers by controlling the amount of impinged air and potentially its temperature.

5 CONCLUSIONS

This work presented a preliminary evaluation of two concepts for tip clearance control in a representative mid-sized turbofan 10-stage axial compressor. Stage 9 was the object of study. Two basic concepts, impingement cooling and heat pipes, as well as the combination of both, were assessed. A finite-element model was created and transient thermo-structural simulations were carried out. Dynamic behavior was not analysed. Concerning validation, qualitative similarity with selected literature results was achieved. No strict validation is possible, due to the lack of experimental data.

The results demonstrate the potential of the combined impingement-heat pipe TCC concept with air supply from the bypass and no added pump. The best investigated configuration (5° pitchwise HP placement + impingement) reduced clearances in up to 0.45% for the rotor and 0.43% for the stator. Considering previous literature works, this could reflect in up 0.9% polytropic efficiency gains. An analysis of the *von-Mises* stresses on the model showed some stress concentration on the holes made to accommodate the heat pipes. However, the combined system does not impact significantly the casing stress field. An artificial increase in the cooling magnitude demonstrated further clearance reduction potential, tending towards saturation, as the heat pipe temperatures decreased.

A transient slam analysis was also performed to preliminarily assess rubbing danger. Although conclusive statements cannot be made, a robust impingement control system can mitigate the severity of clearance pinch points. By simply turning impingement off as the engine decelerates and reaccelerates, 0.24% opening of the actively controlled critical clearance was achieved.

The combined concept was deemed worth of further investigations, given the promising results. Future work is in the process of planning. It aims at assessing and optimizing heat pipe structural integration, and improving cooling. Heat pipe dry-out recuperation and working fluid stability at the high MTO temperature regime remain open issues.

DECLARATION OF COMPETING INTERESTS

The authors declare no conflict of interest of any nature upon the development and publication of this work.

ACKNOWLEDGEMENTS

The authors would like to acknowledge the contribution of the LRZ - Supercomputing Center for providing the required computational resources for this work. A word of gratitude is extended to Mr. Pedro Henrique de Melo Casado Matos, Mr. Ioannis Zaimis and Mrs. Simona Rocchi for the fruitful discussions regarding the present publication.

REFERENCES

[1] S. Lattime and B. Steinetz, "Turbine engine clearance control systems: Current practices and future directions," in *38th AIAA/ASME/SAE/ASEE Joint Propulsion Conference & Exhibit*, ASME, 2002.

[2] E. Kawecki, *Thermal Response Turbine Shroud Study.* Technical Report, Defense Technical Information Center, Fort Belvoir (1979).

[3] J. Schmücker and A. Schäffler, "Performance deterioration of axial compressors due to blade defects," in *Propulsion and Energetics Panel Symposium*, AGARD, 1994.

[4] A. Hupfer, *Spalte in Fluggasturbinen – Ursachen, Folgen und Optimierungsstrategien am Beispiel des Turboverdichters*. Habilitation, Technical University of Munich, 2019.

[5] R. Merkler, S. Staudacher, M. Schölch, H. Schulte, and K.-J. Schmidt, "Simulation of clearance changes and mechanical stresses in transient gas turbine operation by a matrix method," in *41st AIAA/ASME/SAE/ASEE Joint Propulsion Conference & Exhibit*, AIAA, 2005.

[6] H. Schulte, K.-J. Schmidt, A. Weckend, and S. Staudacher, "Multi-stage compressor model for transient performance simulations," in *ASME Turbo Expo: Power for Land, Sea, and Air*, 2008.

[7] A. Weckend, *Stabilitätsbetrachtungen Mittels Stufenweiser Verdichtermodellierung in der Triebwerksleistungsrechnung*. Doctoral thesis, University Stuttgart, 2013.

[8] D. Rockel, S. Weihard, A. Hachmann, A. Hupfer, and H.-P. Kau, "Numerical investigation of an additively manufactured compressor casing: The effect of auxetic structures on the tip clearances," in *Turbo Expo: Power for Land, Sea, and Air*, ASME, 2013.

[9] T. Schmidt, J. Lorenz, V. Gümmer, and A. Hupfer, "Structural analysis of an auxetic casing structure incorporating tip blowing casing treatment modification," in *ASME Turbo Expo 2019: Turbomachinery Technical Conference and Exposition*, ASME, 2019.

[10] J. W. Bae, K. S. Breuer, and C. S. Tan, "Active control of tip clearance flow in axial compressors," *Journal of Turbomachinery*, 2005:127.

[11] A. J. Strazisar, M. M. Bright, S. Thorp, D. E. Culley, and K. L. Suder, "Compressor stall control through endwall recirculation," in *Turbo Expo: Power for Land, Sea, and Air*, 2004.

[12] W. Horn, *Verbesserung des Betriebsverhaltens von Turboflugtriebwerken durch aktiv geregelte Verdichter*. Doctoral thesis, University Stuttgart, 2011.

[13] T. Schmidt, *Implementierung von Metamodellierungsansätzen in der Vorauslegung von Verdichtergehäusekonstruktionen mit Fokus auf Spalthaltung*. Doctoral thesis, Technical University of Munich, 2022.

[14] GasTurb GmbH, *GasTurb 14 - Design and Off-Design Performance of Gas Turbines*. User Guide (2022).

[15] B. K. Sultanian, *Gas Turbines: Internal Flow Systems Modeling*. Cambridge, UK: Cambridge University Press, first ed ed., 2018.

[16] A. Alexiou, N. J. Hills, C. A. Long, A. B. Turner, and J. A. Millward, "Heat transfer in high-pressure compressor gas turbine internal air systems: a rotating disc-cone cavity with axial throughflow," *Experimental Heat Transfer*, 2000:13.

[17] Society of German Engineers (VDI), *VDI Heat Atlas*. Berlin, Heidelberg, DE: Springer, second ed ed., 2010.

[18] T. Schmidt, V. Gümmer, and M. Konle, "Potential of surrogate modelling in compressor casing design focusing on rapid tip clearance assessments," *The Aeronautical Journal*, 2021:125.

[19] J. DeCastro and K. Melcher, "A study on the requirements for fast active turbine tip clearance control systems," in *40th AIAA/ASME/SAE/ASEE Joint Propulsion Conference & Exhibit*, 2004.

[20] T. Schmidt, V. Gümmer, and M. Konle, "Quantification of the effect of circumferential repeated 3d features on radial displacement of a compressor casing focusing model simplification: Part i," in *8th International Conference on Mechanics and Industrial Engineering*, ICMIE, 2019.

[21] R. Brandt, L. Pawlowski, G. Neuer, and P. Fauchais, "Specific heat and thermal conductivity of plasma sprayed yttria-stabilized zirconia and nial, nicr, nicral, nicraly, nicocraly coatings," *High Temperatures. High Pressures (Print)*, 1986:18.

[22] USA Department of Defense, *Military Handbook: Metallic Materials and Elements for Aerospace Vehicle Structures*. Champaign IL, USA: USA Department of Defense, 1990.

[23] J. Davis, *Nickel, Cobalt, and Their Alloys*. Novelty OH, USA: ASM International, 2000.

[24] R. Thompson and K. Hemker, "Thermal expansion measurements on coating materials by digital image correlation," in *Proceedings of the SEM Conference*, 2007.

[25] Special Metals Corporation, "Inconel alloy 718spf technical sheet." www.specialmetals.com, accessed on 03.03.2023.

[26] European Aviation Safety Agency, *Type-Certificate Data Sheet No. E.018 for BR700-710 Engines - Rolls-Royce Deutschland GmbH*. Certification Sheet (2022).

[27] B. P. Keller, S. E. Nelson, K. L. Walton, T. K. Ghosh, R. V. Tompson, and S. K. Loyalka, "Total hemispherical emissivity of inconel 718," *Nuclear Engineering and Design*, 2015:287.

[28] D. Rockel, *Zum Potenzial von additiven Fertigungsverfahren in zukünftigen Triebwerksverdichtern*. Doctoral thesis, Technical University of Munich, 2015.

[29] M. Tirovic and G. Voller, "Interface pressure distributions and thermal contact resistance of a bolted joint," *Proceedings of the Royal Society A: Mathematical, Physical and Engineering Sciences*, 2005:461.

[30] M. Jalalpour, J. Kim, and M. Reda Taha, "Monitoring of l-shape bolted joint tightness using thermal contact resistance," *Experimental Mechanics*, 2013:53.

[31] L. W. Florschuetz, C. R. Truman, and D. E. Metzger, "Streamwise flow and heat transfer distributions for jet array impingement with crossflow," *Journal of Heat Transfer*, 1981:103.

[32] M. Goodro, P. Ligrani, M. Fox, and H.-K. Moon, "Mach number, reynolds number, jet spacing variations: Full array of impinging jets," *Journal of Thermophysics and Heat Transfer*, 2010:24.

[33] F. Ben Ahmed, B. Weigand, and K. Meier, "Heat transfer and pressure drop characteristics for a turbine casing impingement cooling system," in *International Heat Transfer Conference*, ASME, 2010.

[34] J. Zhao, Y. Ji, D.-Z. Yuan, Y.-X. Guo, and S.-W. Zhou, "Structural effect of internal composite wick on the anti-gravity heat transfer performance of a concentric annular high-temperature heat pipe," *International Communications in Heat and Mass Transfer*, 2022:139.

[35] H. Noda, K. Yoshioka, and T. Hamatake, "An experimental study on the permeability of screen wicks," *JSME International Journal Series B*, 1993:36.

[36] S. Chi, *Heat Pipe Theory and Practice: A Sourcebook*. Washington DC, USA: Hemisphere Publishing Corporation, first ed ed., 1976.

[37] A. Faghri, *Heat Pipe Science And Technology*. Washington DC, USA: Taylor & Francis, first ed ed., 1995.

[38] P. Nemec, A. Čaja, and M. Malcho, "Mathematical model for heat transfer limitations of heat pipe," *Mathematical and Computer Modelling*, 2013:57.

[39] A. Faghri and Y. Zhang, *Transport Phenomena in Multiphase Systems*. Burlington MA, USA: Elsevier, first ed., 2006.

[40] F. A., Z. Y., and H. J., *Advanced Heat and Mass Transfer*. Columbia MO, USA: Global Digital Press, first ed., 2010.

[41] S. Eisenmann, M. Mair, and A. Hupfer, "Structural analysis of a gas turbine disk containing heat pipes using finite element analysis," in *50th AIAA/ASME/SAE/ASEE Joint Propulsion Conference*, AIAA, 2014.

[42] K. Baraya, J. A. Weibel, and S. V. Garimella, "Heat pipe dryout and temperature hysteresis in response to transient heat pulses exceeding the capillary limit," *International Journal of Heat and Mass Transfer*, 2020:148.